JOURNAL OF Applied Polymer SCIENCE

Preparation and Characterization of Surface Modified Silicon Carbide/Polystyrene Nanocomposites

Jian-Ping Cao,[1] Jun Zhao,[1] Xiaodong Zhao,[1] Guo-Hua Hu,[2] Zhi-Min Dang[1]

[1]Department of Polymer Science and Engineering, School of Chemistry and Biological Engineering, University of Science and Technology Beijing, Beijing 100083, People's Republic of China

[2]CNRS-Universté de Lorraine, Laboratoire Réactions et Génie des Procédés, UPR3349, ENSIC, 1 rue Grandville, BP 20451, Nancy, F-54000, France

Correspondence to: Z.-M. Dang (E-mail: dangzm@ustb.edu.cn) or G.-H. Hu (E-mail: guo-hua.hu@univ-lorraine.fr)

ABSTRACT: A simple method is reported to coat silicon carbide (SiC) nanoparticles with polystyrene (PS) to improve the interfacial adhesion between polymer matrix and SiC nanoparticles. The morphology of untreated SiC nanoparticles, PS coated SiC (*p*-SiC) nanoparticles, SiC/PS nanocomposites, and *p*-SiC/PS nanocomposites are observed. The HRTEM image of *p*-SiC shows that the thickness of PS on the surface of SiC is about 1.5–2.0 nm, which is consistent with the TGA results. With 24.7 vol % untreated SiC nanoparticles dispersed into PS matrix, the thermal conductivity (λ) of the SiC/PS composites increases by about 192%. However, when the same volume fraction of *p*-SiC nanoparticles is used, the increase is about 353%. This big difference could be attributed to the promoted dispersion of the *p*-SiC in the PS matrix. The measurements of glass transition (T_g), dielectric constant (ε), and tensile strength at break (σ_b) also support this explanation. © 2013 Wiley Periodicals, Inc. J. Appl. Polym. Sci. 130: 638–644, 2013

KEYWORDS: composites; polystyrene; thermal properties; dielectric properties; surfaces and interfaces

Received 19 December 2012; accepted 17 February 2013; published online 2 April 2013
DOI: 10.1002/app.39186

INTRODUCTION

Polymeric materials have attracted much attention because of their low density, easy processing, and wide range of applications. However, the intrinsic thermal conductivity and dielectric constant of the polymers is low, which limits their application as microwave dielectrics and the power energy storage materials.[1,2] A thermally conductive and dielectric composite can be manufactured by adding ceramic fillers with high thermal conductivity and high dielectric constant into the polymer matrix.[3–5]

It has been reported that reducing the modulus mismatch between polymer matrix and solid fillers and promoting the dispersion of the fillers in the polymer matrix could improve the thermal conductivity and dielectric properties of the polymer composites.[6–9] One method to reduce the modulus mismatch and promote the dispersion is the surface treatment of fillers,[10–12] for example, by silane treatment, which could significantly improve the heat transfer capability of the composites. Another useful method is to coat the fillers surface with a thin layer of polymer, which is compatible with the matrix.[13]

The coating can be obtained via a process called adsorption polymerization in which the polymerization takes place in a surfactant bilayer adsorbed on the substrate surface.[14,15] The resulting polymer layer in nanoscale is very uniform. The process has been successfully used to coat a thin polymeric layer on a wide range of inorganic substrates, including boron nitride,[16] silica,[17] and alumina.[18] It has also been used to improve the adhesion between the fillers and matrix to acquire high mechanical strength of the composites.[19] However, the application of the process to improve the heat transfer of particulate-filled composites is relatively few.[20]

Polystyrene (PS) composites including nanocomposites have gained wide applications in different branches of industry because of their low cost, low density, chemical inertia, and low thermal conductivity.[21,22] However, the dielectric constant and thermal conductivity of PS is very low. In some applications, especially as electrical and electronic packaging materials, high thermal conductivity is needed to dissipate heat, and maintain operating temperature.[2] Silicon carbide (SiC) is a nonoxide semiconductor ceramic material with many excellent properties, such as high thermal conductivity, passivity to reactions with acids and melts, superb oxidation resistance, excellent thermal shock resistance, and extremely high hardness, which make it widely used in microwave dielectrics and the power energy storage materials.[23,24] But, the SiC nanoparticles are very easy to agglomerate which will influence the physicochemical properties

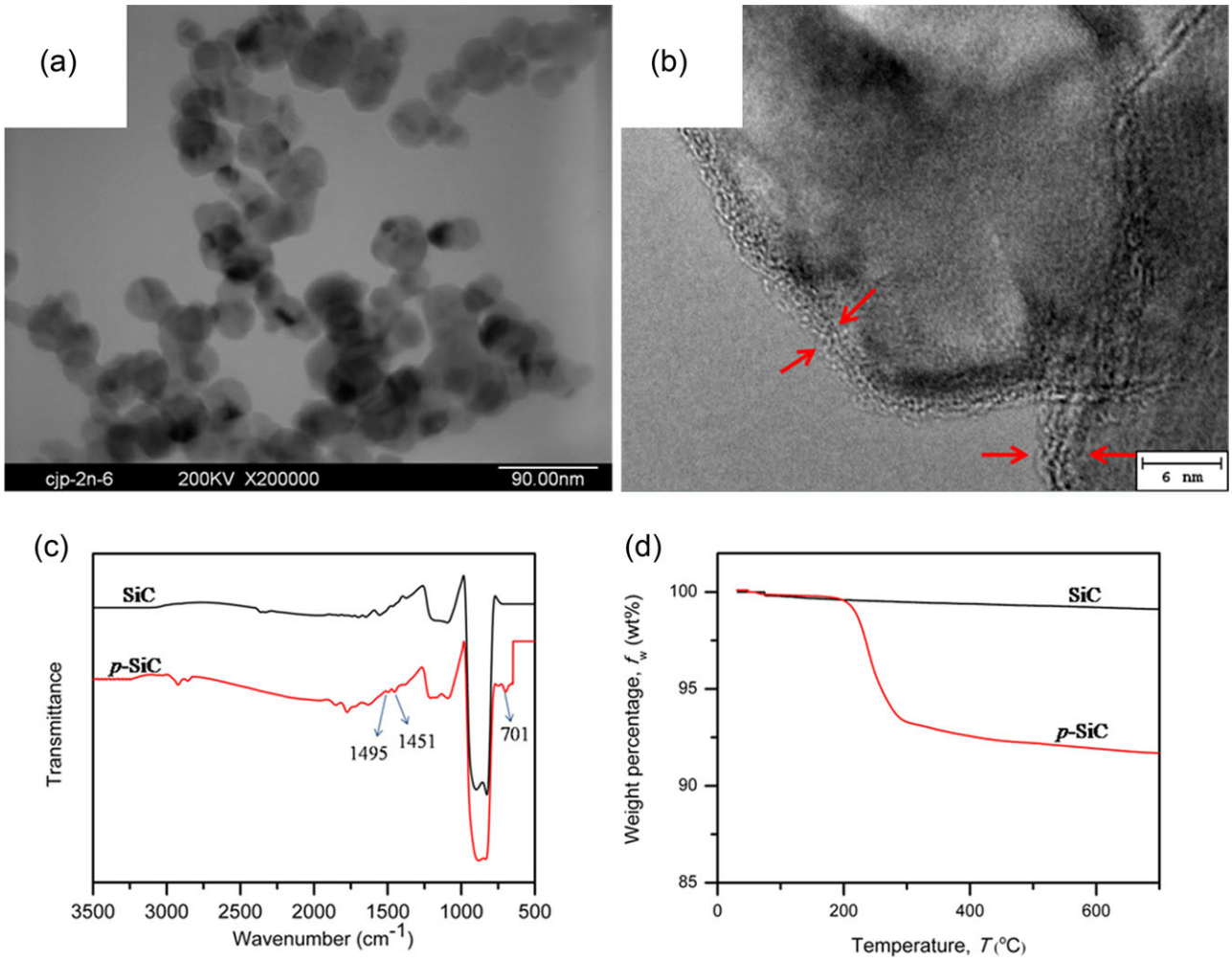

Figure 1. (a) TEM image of SiC nanoparticles, (b) HRTEM image of *p*-SiC nanoparticles, (c) FTIR spectra of SiC and *p*-SiC, and (d) TGA curves of SiC and *p*-SiC. [Color figure can be viewed in the online issue, which is available at wileyonlinelibrary.com.]

of the composites.[25–29] Therefore, it is possible to achieve high performance of the composites by surface modification of SiC nanoparticles. In this work, a series of PS composites will be fabricated by using raw SiC and PS coated SiC (*p*-SiC) nanoparticles, respectively. The effect of fillers' surface treatments on the morphology, thermal properties, dielectric properties, and mechanical properties of the composites will be systematically investigated.

EXPERIMENTAL

Materials

PS pellets (PS-666D) with melt flow rate of 8 g (10 min)$^{-1}$ and density of 1.05 g cm^{-3} was received from Sinopec Beijing Yanshan Company (Beijing, China). SiC powders with average diameter of 40 nm and density of 3.2 g cm^{-3} were supplied by Hefei Kaier Nanometer Energy and Technology (Anhui, China). Potassium persulfate ($K_2S_2O_8$) and absolute ethyl alcohol were obtained from Beijing Chemical Plant (Beijing, China). Cetylpyridinium chloride (CPC) was purchased from Sinopharm Chemical Reagent (Beijing, China). Styrene was supplied by Tianjin Fuchen Chemical Reagent Factory (Tianjin, China).

Preparation of *p*-SiC Nanoparticles and PS Nanocomposites

To reduce the agglomeration of SiC nanoparticles, styrene was used to coat the SiC nanoparticles. The synthesis of *p*-SiC was carried out by two steps. First, 5 g SiC particles were added into 100 mL aqueous solution containing 0.35 g CPC surfactant under magnetic stirring for 30 min. Then 0.5 g styrene was added to the solution and the stirring was run at 30°C for 24 h to allow for the adsorption of styrene onto the surface of SiC. The second step was to add 0.03 g $K_2S_2O_8$, raise the temperature to 60°C, and then keep isothermal for 24 h to initiate the polymerization reaction. Afterwards, the obtained *p*-SiC nanoparticles were washed several times with water and ethanol at room temperature. Finally, the samples were dried in an oven at 60°C. To prepare the nanocomposites, the raw SiC and *p*-SiC particles obtained above were directly mixed with PS in a Haake mixer (Germany) at 175°C and 100 rpm for 15 min. The obtained mixtures were cooled in air to room temperature.

Characterization

The chemical structure of the SiC and *p*-SiC was characterized by KBr disc method with a Fourier transform infrared (FTIR) spectrometer (Thermo Nicolet 6700) over the range of

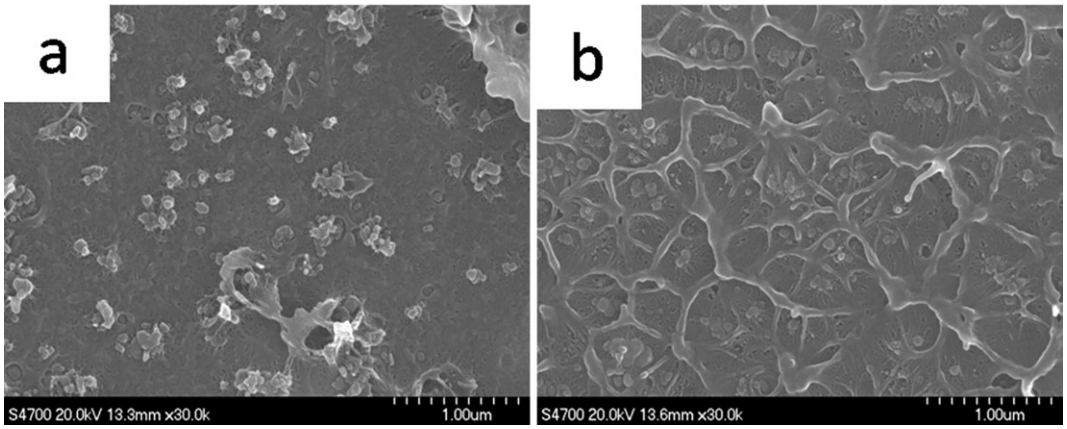

Figure 2. SEM images of (a) SiC/PS nanocomposite and (b) *p*-SiC/PS nanocomposite with a filler content of 7.6 vol %.

3500–500 cm^{-1}. Transmission electron microscopy (TEM) and high resolution transmission electron microscope (HRTEM) images were obtained from a Hitachi H7650 instrument and JEOL J-3010 operating at an accelerating voltage of 200 and 300 kV, respectively. Dilute solutions of nanoparticles were dropped onto carbon-coated copper grids and dried completely in air for measurements. Scanning electron microscopy (SEM) was conducted on a Hitachi S4700 instrument at room temperature to observe the dispersion of untreated SiC and *p*-SiC nanoparticles in the matrix. The prepared nanocomposite samples were fractured in liquid nitrogen, and the fracture surface was sputtered with a thin layer of gold to avoid the accumulation of charge during SEM measurements.

Thermal gravimetric analysis (TGA) measurements were performed on a SDT Q600 analyzer (TA instruments, New Castle) with the sample mass of 5–10 mg and a heating rate of 10 K min^{-1} under nitrogen protection. Differential scanning calorimetry (DSC) was performed on a DSC-60 (Shimadzu corporation, Japan) to measure the glass transition temperature (T_g) of nanocomposites. The samples were heated from 30 to 180°C at 10 K min^{-1} in nitrogen atmosphere.

The thermal conductivity of the composites was measured on a HC-074 heat flow meter instrument (EKO Instrument Sirading, Germany) according to ASTM D5470. The obtained nanocomposites were compression molded into plates at 190°C for 15 min and then at room temperature for 15 min under a pressure of 20 MPa. Samples were prepared in cylindrical shape with diameter of about 55.0 mm and thickness of about 4.0 mm. Each point in figure was the average value of three experimental points.

Samples of cylindrical shape with circle area of about 1.0 cm^2 and thickness of about 1.0 mm for dielectric measurements were molded by hot pressing at 195°C and 20 MPa for 10 min. Both sides of the samples were coated with silver as electrodes. The dielectric measurements were performed on an Agilent 4294A Impedance Analyzer (USA) over the frequency range of 10^2–10^7 Hz. The electrical resistivity at room temperature was measured in the thickness direction of the composite films using a Keithley 6517B picoammeter Voltage Source with diameter of about 55.0 mm and thickness of about 1.0 mm. One data point was the average value of six experimental points. Injection molding on a HAAKE Mini Jet II (Thermo scientific, Germany) was used to prepare the samples for tensile tests. The

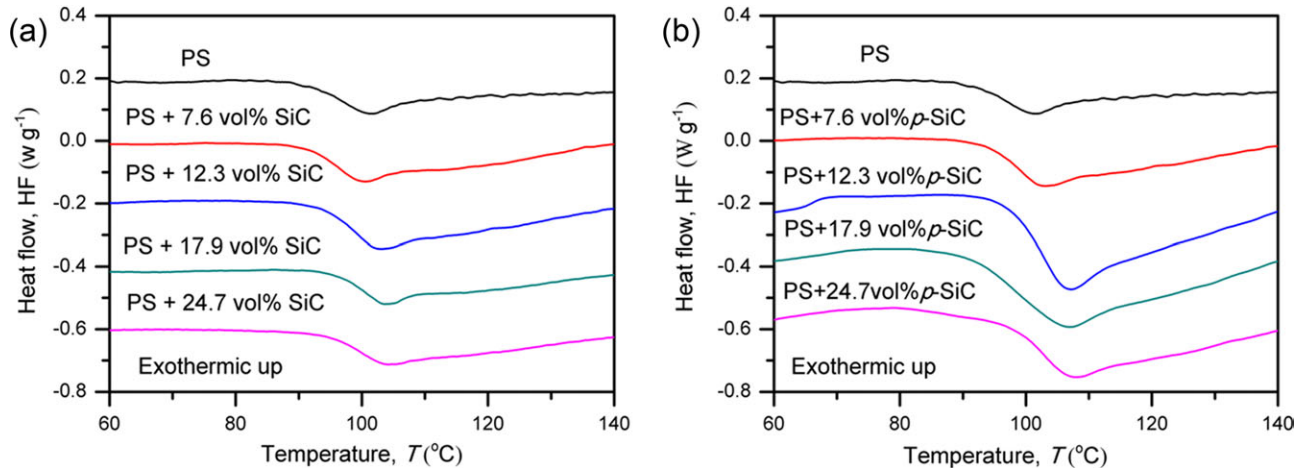

Figure 3. DSC heating curves of (a) SiC/PS and (b) *p*-SiC/PS nanocomposites. [Color figure can be viewed in the online issue, which is available at wileyonlinelibrary.com.]

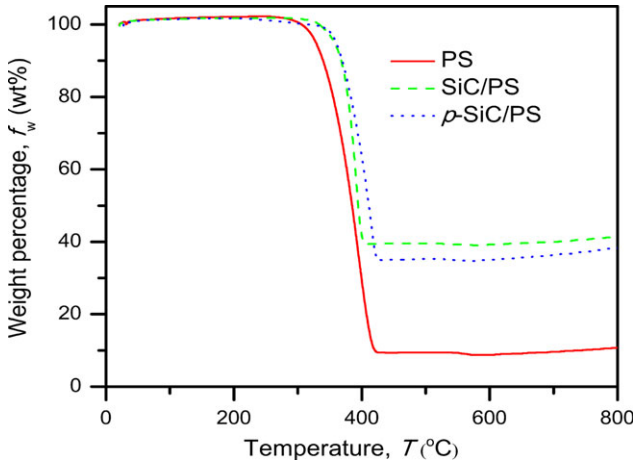

Figure 4. TGA curves of pure PS, SiC/PS nanocomposites, and *p*-SiC/PS nanocomposites with 12.3 vol % fillers. [Color figure can be viewed in the online issue, which is available at wileyonlinelibrary.com.]

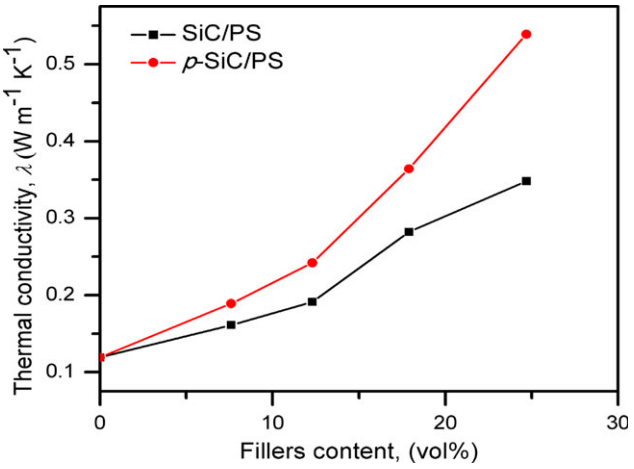

Figure 6. Effect of the volume fraction of SiC and *p*-SiC fillers on the λ of their PS composites. The lines are the guide to the eyes. The composites with 0 vol % fillers means PS matrix. [Color figure can be viewed in the online issue, which is available at wileyonlinelibrary.com.]

injection temperature and pressure were 195°C and 75 GPa, respectively. The holding temperature and time were 78°C and 8 s, respectively. Tensile testing was performed based on ASTM D638-10 using at least five samples to ensure good measurement statistics. The testing was performed on an AG-IC 50KN tensile tester (Shimadzu Corporation, Japan) with a cross head speed of 10 mm min^{-1} at room temperature. The initial clamp distance was 30.0 mm. The samples' thickness was 1.0 mm and the width was 4.0 mm. The stress at break (σ_b) was recorded. The value of mechanical properties was calculated using at least five samples with the same composition.

RESULTS AND DISCUSSION

Characterization of Nanoparticles

Figure 1 shows the characterization of SiC and *p*-SiC nanoparticles. As can be seen from Figure 1(a), the SiC nanoparticles are approximately spherical and possessed an average diameter of about 40 nm. HRTEM image of *p*-SiC provides visual evidence of the PS coating on the surface of SiC nanoparticles. The coating is very uniform, as shown in Figure 1(b) marked with arrows, and the thickness of the PS coating was ~1.5–2.0 nm. The FTIR spectra of SiC and *p*-SiC nanoparticles are shown in Figure 1(c). The broad band at 750–1000 cm^{-1} is assigned to Si—C stretching vibration. For the *p*-SiC, two characteristic peaks of PS at 1495 and 1451 cm^{-1} assigned to aromatic C=C stretching, and a peak at 701 cm^{-1} assigned to out-of-plane aromatic C—H bending can be seen. The results confirm that PS was successfully coated on the SiC particles by polymerization. Figure 1(d) shows the TGA curves of SiC and *p*-SiC nanoparticles within the experimental temperature range (30–700°C). The SiC has nearly no thermal degradation process while the *p*-SiC has one mass loss step and the initial decomposition temperature is about 200.1°C. The amount of residual carbon was about 91.7 wt %, by which the wrapping ratio of PS on the surface of SiC core for *p*-SiC can be calculated to be about 8.3 wt %, corresponding to an average thickness of about 1.8 nm. This result is consistent with the HRTEM image of *p*-SiC as shown in Figure 1(b).

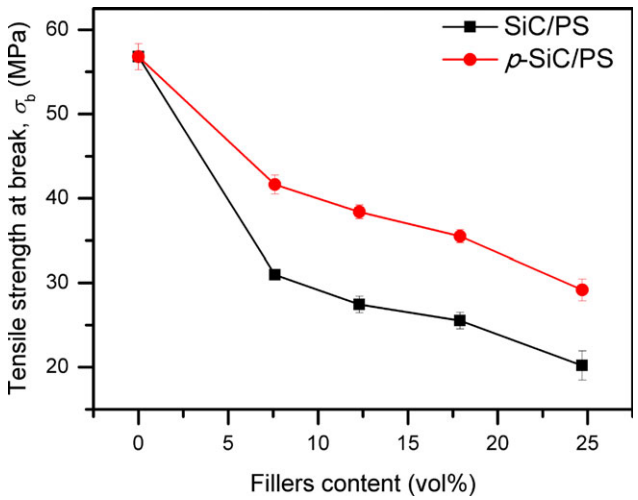

Figure 5. The σ_b of SiC/PS and *p*-SiC/PS nanocomposites with various concentrations of fillers. The lines are the guide to the eyes. The composites with 0 vol % fillers means PS matrix. [Color figure can be viewed in the online issue, which is available at wileyonlinelibrary.com.]

Morphology of the Composites

Figure 2 shows the SEM images of SiC/PS and *p*-SiC/PS nanocomposites with 7.6 vol % fillers. It can be seen that the fracture surface of SiC/PS and *p*-SiC/PS composites revealed obviously different features. The fracture surface of the SiC/PS composites is smoother than that of the PS/*p*-SiC composites. Actually, the surface of the latter forms protruded network, which is a typical characteristic of ductile breakage[30] because of the matching modulus between the *p*-SiC nanoparticles and PS matrix. These results indicate that the interfacial interaction between PS matrix and *p*-SiC was stronger than that between PS and SiC. Moreover, large SiC nanoparticles agglomerates can be clearly seen in the SEM images. However, for *p*-SiC/PS nanocomposite, the size of the aggregates was significantly reduced,

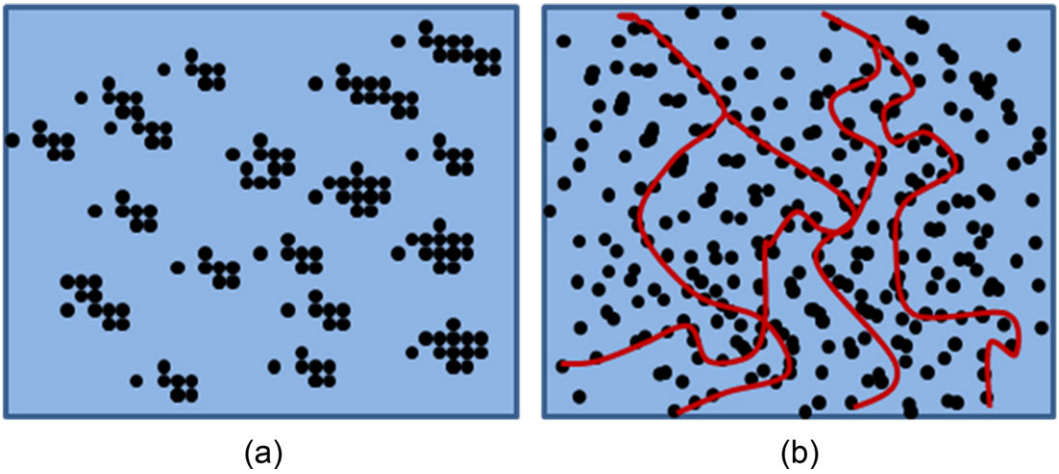

Figure 7. Schematic illustration of the particles dispersion in (a) SiC/PS and (b) *p*-SiC/PS nanocomposites. [Color figure can be viewed in the online issue, which is available at wileyonlinelibrary.com.]

confirming that the dispersion of nanoparticles was enhanced remarkably due to the PS coating on the surface of SiC core for *p*-SiC.

Thermal Properties of the Composites

Figure 3 shows the DSC curves of SiC/PS and *p*-SiC/PS nanocomposites. It can be seen from Figure 3(c) that the glass transition temperature (T_g) of the composites increased with increasing content of nanoparticles. The T_g of the composites increased by 3.4°C for 24.7 vol % SiC, while it increased by 6.7°C for the same content of *p*-SiC nanoparticles. The increase in T_g with the addition of SiC nanoparticles indicates that the nanoparticles can act as physical interlock points in the nanocomposites, which generally restrains the polymer chain mobility.[31] The T_g of the *p*-SiC/PS composites was higher than that of SiC/PS composites for the same filler content, which could be attributed to the stronger interaction between the fillers and the matrix in the former.[13] The PS chains of the surface of *p*-SiC could form strong interface with PS matrix and so the fillers can more effectively restrict the motion of the matrix chains.

Figure 4 shows the TGA curves of pure PS, SiC/PS nanocomposites and *p*-SiC/PS nanocomposites with the fillers' concentration of 12.3 vol % (corresponding to 30 wt %). Within the experimental temperature range (20–800°C), the thermal degradation process apparently presents a single mass loss step for PS and SiC/PS samples. However, there is a small degradation stage between 200 and 350°C with 2.0 wt % percent of weight loss before the matrix degradation. It should attribute to the decomposition of the coating PS at SiC surface, which is consistent with Figure 1(d). It can be seen that the initial decomposition temperature of pure PS was about 306.7°C while those of the SiC/PS and *p*-SiC/PS nanocomposite were about 334.0°C and about 349.2°C, respectively. This indicates that both the SiC and *p*-SiC nanoparticles could improve the thermal stability of PS matrix. According to Figure 4, the amount of residual carbon was about 10.8, 41.3, and 39.0 wt % for pure PS, SiC/PS nanocomposite, and *p*-SiC/PS nanocomposite, respectively. This difference is due to the existence of inorganic SiC. The amount of residual carbon of *p*-SiC/PS nanocomposite was 2.3 wt % lower than that of SiC/PS nanocomposite with 30 wt % filler content, which also provides an evidence of the successful polymerization of styrene molecules on the surface of SiC nanoplaticles.[32] According to this difference, the PS thickness on the SiC surface for the *p*-SiC nanoparticles is about 1.79 nm, which is in agreement with the results shown in Figure 1.

Mechanical Properties

Figure 5 shows the tensile strength at break (σ_b) of SiC/PS and *p*-SiC/PS nanocomposites filled with various concentrations of fillers. The σ_b of both nanocomposites decreased with increasing content of fillers. The nanoparticles introduce a small cap shaped cavity and this cavity will induce extra stress concentration in the vicinity of its relatively sharp edge.[33] Thus, craze formation at the edge of the cavity occurs at a lower applied stress. However, the σ_b of the *p*-SiC/PS composites was a little higher than that of SiC/PS composites. It means the PS modification could increase the interfacial interaction between fillers and matrix and improve the dispersion of SiC in the PS matrix. This is consistent with the DSC results shown above.

Thermal Conductivity and Dielectric Properties

Figure 6 shows the effect of the volume fraction of SiC and *p*-SiC fillers on the thermal conductivity (λ) of the nanocomposites. It can be seen that the λ was remarkably increased with increasing amount of both raw SiC and *p*-SiC nanoparticles. The λ of pure PS was about 0.119 W m^{-1} K^{-1}. For the addition of 24.7 vol % fillers, it increased from 0.348 to 0.539 W m^{-1} K^{-1} for the raw SiC and *p*-SiC nanocomposites, respectively. The increase was about 192 and 353%, respectively. When the filler content was lower than 12.3 vol %, the increase of λ was relatively smaller because the nanoparticles could not contact each other. However, with further increasing filler content, the particles began to contact each other and gradually formed three-dimensional heat conduction network. Therefore, the λ of the samples was increased more significantly.

It can be seen from Figure 6 that the enhancement of λ by the same loading of untreated SiC was lower than that by the *p*-SiC. To understand this, a schematic illustration of the

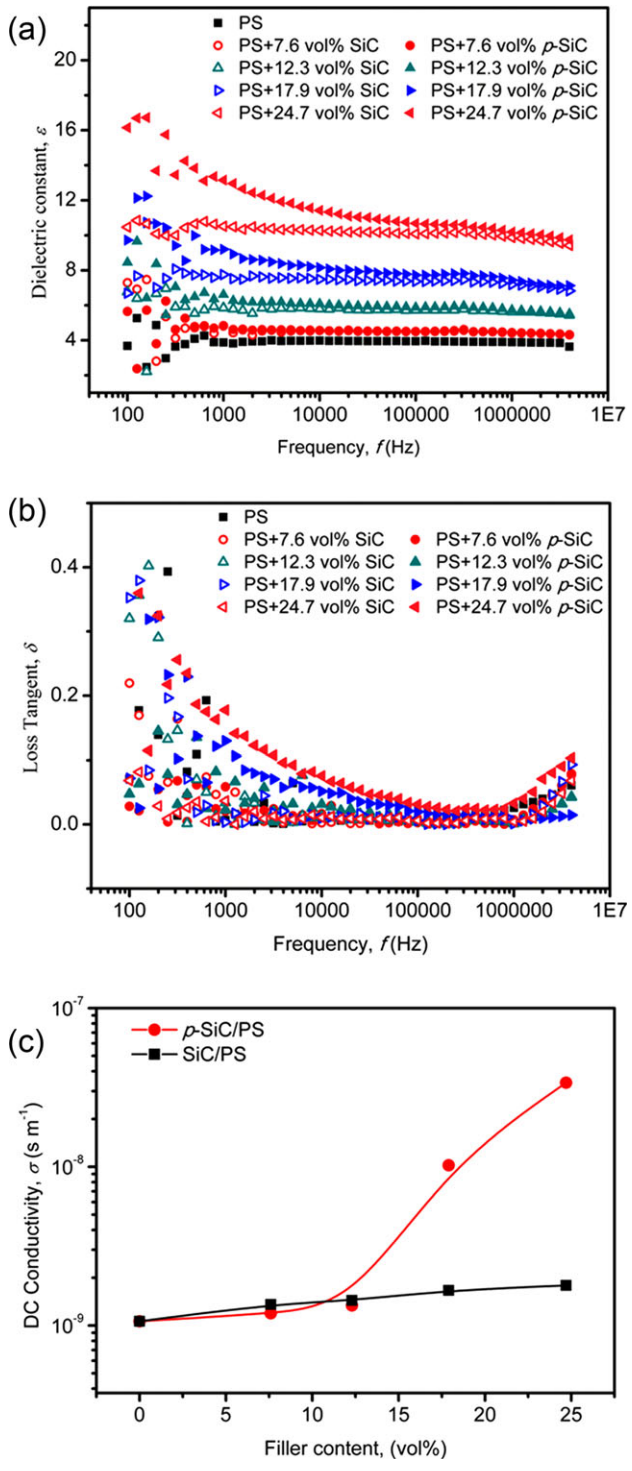

Figure 8. Frequency dependences of (a) ε and (b) loss tangent, (c) DC conductivity of SiC/PS and *p*-SiC composites with various volume fraction of filler. [Color figure can be viewed in the online issue, which is available at wileyonlinelibrary.com.]

particles dispersion is proposed in Figure 7. The untreated SiC nanoparticles were very easy to agglomerate. Hence, the heat transport network cannot be formed effectively at the same volume of filler according to Figure 7(a). However, the coating modification provided good interface compatibility between the SiC surface and the polymer matrix which allowed SiC to disperse well in the PS matrix. So, the *p*-SiC particles could easily form the heat transport network according to Figure 7(b). A homogeneous SiC network could effectively form the heat transport network and promote the diffusion of phonon in the SiC/PS nanocomposites.

Figure 8 presents the dielectric properties of the SiC/PS and *p*-SiC/PS nanocomposites with various filler concentrations. The ε of the PS matrix was all remarkably increased by adding both SiC and *p*-SiC fillers and the ε of *p*-SiC/PS composites was higher than that of SiC/PS composites for the same volume fraction of fillers [as shown in Figure 8(a)]. This phenomenon was because that the weaker interfacial interaction in SiC/PS composite lead to more voids in the composites. The voids were filled with air, and the dielectric constant of air was very low (about 1), which would make the composite material exhibit a lower dielectric constant. According to the microcapacitor theory, good dispersion of SiC means more microcapacitors exists in p-SiC/PS nanocomposites, so ε is higher than SiC/PS. Figure 8(b) shows the frequency dependence of the loss tangent of the SiC/PS and *p*-SiC/PS nanocomposites with various filler concentrations. It can be seen that the loss tangent of *p*-SiC/PS nanocomposites are all higher than the SiC/PS nanocomposites. Because of the better dispersion of *p*-SiC in the PS matrix, there was more network exist as illustrate in Figure 7. As a result, the conductivity loss is higher than SiC/PS nanocomposites, so the loss tangent is higher than SiC/PS nanocomposites. In addition, this point is demonstrated by Figure 8(c), as the volume fraction of filler increase, the direct current (DC) conductivity of *p*-SiC/PS nanocomposites is higher than SiC/PS nanocomposites. It is also explained that why the λ of *p*-SiC/PS nanocomposites is higher than SiC/PS nanocomposites.

CONCLUSIONS

SiC particles were coated with PS by adsorption polymerization successfully. The wrapping ratio and thickness of the coating were about 8.3 wt % and 1–2 nm, respectively. The coating of SiC nanopaticles with PS improved the interaction between the fillers and the matrix and resulted in better dispersion of nanoparticles in the matrix. Compared with the SiC/PS, the *p*-SiC/PS nanocomposites exhibited high thermal conductivity (~0.54 W m^{-1} K^{-1}) and high dielectric constant (15) at 100 Hz. Our findings could help understand the effect of interface interaction between fillers and polymer matrix on the thermal and dielectric properties of polymer nanocomposites.

ACKNOWLEDGMENTS

This work was financially supported by NSF of China (Grant Nos. 50977001 and 51073015), State Key Laboratory of Power System (SKLD11KZ04), the Fundamental Research Funds for the Central Universities (Nos. 06103012 and 06103011), and Beijing Municipal Excellent Scholars (2011D009006000005). The authors also acknowledge Prof. Rui Song of Graduate University of Chinese Academy of Sciences for his assistance in TGA measurements.

REFERENCES

1. Ganguli, S.; Roy, A. K.; Anderson, D. P. *Carbon* **2008**, *46*, 80.
2. He, H.; Fu, R.; Shen, Y.; Han, Y. C.; Song, X. F. *Compos. Sci. Technol.* **2007**, *67*, 2493.
3. Li, Y.; Huang, X. Y.; Hu, Z. W.; Jiang, P. K.; Li, S. T.; Tanaka, T. *ACS Appl. Mater. Int.* **2011**, *3*, 4396.
4. Li, T. L.; Hsu, S. L. C. *J. Phys. Chem. B.* **2010**, *114*, 6825.
5. Veca, L. M.; Meziani, M. J.; Wang, W.; Wang, X.; Lu, F. S.; Zhang, P. Y.; Lin, Y.; Fee, R.; Connell, J. W.; Sun, Y. P. *Adv. Mater.* **2009**, *21*, 2088.
6. Xie, X. L.; Mai, Y. W.; Zhou, X. P. *Mater. Sci. Eng. Rep.* **2005**, *49*, 89.
7. Peters, J. E.; Papavassiliou, D. V.; Grady, B. P. *Macromolecules* **2008**, *41*, 7274.
8. Hu, M.; Shenogin, S.; Keblinski, P. *Appl. Phys. Lett.* **2007**, *91*, 2419100.
9. Hu, M.; Keblinski, P.; Schelling, P. K. *Phys. Rev. B* **2009**, *79*, 1043051.
10. Abdalla, M.; Dean, D.; Robinson, P.; Nyairo, E. *Polymer* **2008**, *49*, 3310.
11. Bagwe, R. P.; Hilliard, L. R.; Tan, W. H. *Langmuir* **2006**, *22*, 4357.
12. Abdelmouleh, M.; Boufi, S.; Belgacem, M. N.; Duarte, A. P.; Ben S. A.; Gandini, A. *Int. J. Adhes. Adhes.* **2004**, *24*, 43.
13. Yu, J.; Huang, X.; Wu, C.; Wu, X.; Wang, G.; Jiang, P. *Polymer* **2012**, *53*, 471.
14. Strankowski, M.; Strankowska, J.; Gazda, M.; Piszczyk, L.; Nowaczyk, G.; Jurga, S. *Express. Polym. Lett.* **2012**, *6*, 610.
15. Wang, S.; Russo, T.; Qiao, G. G.; Solomon, D. H.; Shanks, R. A. *J. Mater. Sci.* **2006**, *41*, 7474.
16. Wattanakul, K.; Manuspiya, H.; Yanumet, N. *J. Appl. Polym. Sci.* **2011**, *119*, 3234.
17. Jain, S.; Goossens, H.; Picchioni, F.; Magusin, P.; Mezari, B.; Duin, M. *Polymer* **2005**, *46*, 6666.
18. Karlsson, P. M.; Esbjornsson, N. B.; Holmberg, K. *J. Colloid. Interf. Sci.* **2009**, *337*, 364.
19. Sangthong, S.; Pongprayoon, T.; Yanumet, N. *Compos. A.* **2009**, *40*, 687.
20. Zhou, T.; Wang, X.; Gu, M.; Liu, X. *Polymer* **2008**, *49*, 4666.
21. Martins, J. A.; Cruz, V. S. *Polymer* **2011**, *52*, 5149.
22. Cailiang, Z.; Bin, Z.; Lee, L. J. *Polymer* **2011**, *52*, 1847.
23. Zhou, W. Y.; Yu, D, M.; Min, C.; Fu, Y. P; Guo, X. S. *J. Appl. Polym. Sci.* **2009**, *112*, 1695.
24. Philip, P.; Jitka, S. *IEEE Trans. Compon. Hybr. Manuf. Technol.* **1991**, *14*, 835.
25. Karul, A.; Tan, K. T.; White, C. C.; Hunston, D. L.; Marshall, S. T. Akgun, B.; Satija, S. K; Soles, C. L; Vogt, B. D. *Polymer* **2009**, *50*, 3234.
26. Bhattacharya, M.; Bhowmick, A. K. *Polymer* **2008**, *49*, 4808.
27. Korzhenko, A.; Tabellout, M.; Emery, J. R. *Polymer* **1999**, *40*, 7187.
28. Lei, Y.; Tang, Z.; Zhu, L.; Guo, B.; Jia, D. *Polymer* **2011**, *52*, 1337.
29. Tao, F.; Nysten, B.; Baudouin, A. C.; Thomassin, J. M.; Vuluga, D.; Detrembleur, C.; Bailly, C. *Polymer* **2011**, *52*, 4798.
30. Zhou, T.; Zha, J. W.; Cui, R. Y.; Fan, B. H.; Yuan, J. K.; Dang, Z. M. *ACS Appl. Mater. Int.* **2011**, *3*, 2184.
31. Liu, Y.; Zeng, K.; Zheng, S. *React. Funct. Polym.* **2007**, *67*, 627.
32. Xu, Z. Z.; Wang, C. C.; Yang, W. L.; Deng, Y. H.; Fu, S. K. *J. Magn. Magn. Mater.* **2004**, *277*, 136.
33. Dekkers, M. E. J.; Heikens, D. *J. Mater. Sci.* **1983**, *18*, 3281.